Quantitative multi-parametric assessment of a radiation-induced encepholodysplasia CNS model using magnetic resonance imaging

S. Saito[1,2], K. Sawada[3], X-Z. Sun[4], K-H. Chuang[5], T. Suhara[4], I. Kanno[4], and I. Aoki[4]

[1]Tohoku Univeristy, Sendai, Miyagi, Japan, [2]National Institute of Radiological Sciences, Chiba, Chiba, Japan, [3]Tsukuba International University, [4]National Institute of Radiological Sciences, [5]Singapore Bioimaging Consortium

INTRODUCTION

Radiological examinations, such as abdominal x-ray or CT, during pregnancy have been associated with a slightly increased risk of brain tumor [1]. Radiation exposure during the embryonic period causes various diseases such as hydrocephalus, microcephaly and other brain disorder [2]. Recently, it has been demonstrated that manganese-enhanced MRI (MEMRI), using a $MnCl_2$ contrast agent, can be used to visualize neuro-architecture [3]. MEMRI may also be useful in the evaluation of radiation-induced central nervous system (CNS) disorder. In this study, we non-invasively assessed developmental CNS disorder induced by prenatal x-ray exposure with quantitative MRI. Changes in longitudinal relaxation time (T_1) induced by intracellular Mn^{2+} contrast agents were quantitatively observed in the CNS of normal and radiation-exposed rats. The apparent diffusion coefficient (ADC) and transverse relaxation time (T_2) were also assessed. A histological study with Hematoxylin-Eosin (cell density and necrotic changing), Activated Caspase-3 (apoptotic changing), and Glial fibrillary acidic protein (astrogliosis) was also performed to evaluate tissue/cellular degeneration.

MATERIALS AND METHODS

Pregnant SD female rats (n = 4, 250~280 g. Japan SLC, Hamamatsu, Japan) were randomly divided into two groups. One group was exposed to a single dose of whole-body x-ray radiation (1.5 Gy) on day-15 of pregnancy. The X-ray irradiation conditions were 200kVp, 20mA, 0.5 mm Cu + 0.5 mm Al filter, 110cm distance from focus to object and 0.27~0.28 Gy/minute dose rate [4]. Two weeks after birth, 10 neonatal male rats were randomly picked from the normal (n = 5, 2WN group) and the radiation-exposed (n = 5, 2WR group) animals. $MnCl_2$ (0.002 ml/g, 50 mM, Sigma-Aldrich) was slowly infused 24 hours before MRI acquisition. Coronal multi-slice T_1-weighted MR images (multi slice SE, TR/TE = 400/9.57 ms, slice thickness = 1.0 mm, matrix = 256*256, field of view = 25.6 * 25.6 mm^2, average = 4), T_1-mapping (2D Look-Locker, TR/TE = 10000/10 ms, slice thickness = 1.0 mm, matrix = 64*32, field of view = 25.6*12.8 mm^2, average = 1), diffusion imaging and T_2-mapping were acquired using a 7.0 T-MRI (Magnet: Kobelco + JASTEC, Japan. Console: Bruker Biospin, Germany) in combination with a volume coil for transmission (Bruker) and 2ch phased array coil for reception (Rapid Biomedical, Germany). T_2-mapping was performed using a multislice SE sequence (slice thickness = 1 mm; FOV = 25.6 × 25.6 mm^2; matrix = 128 × 128; number of repetitions = 1; TR = 3000 ms) with echo-times ranging from 10 to 140 ms in steps of 10ms. Diffusion imaging was performed using SE multi-shoot echo planar imaging (slice thickness = 1 mm; field of view = 25.6 × 25.6 mm^2; matrix = 128 × 128; number of repetitions = 1; TR = 3000 ms; TE = 33 ms). ADC maps were calculated from diffusion-weighted images acquired at six b-values (b = 0, 250, 500, 750, 1000, 1250 s/mm^2, δ= 3ms, Δ= 23ms). After the MRI experiments, all rats were prepared under anesthesia for histology using paraformaldehyde perfusion. To evaluate T_1, a cortical region-of-interest (ROI) was defined on the MEMRI at a position approximately -1.0 mm posterior to the Bregma. Statistical analysis was performed using 2-way ANOVA and an unpaired t-test (*:P<0.05, **:P<0.01, ***:P<0.001).

RESULTS and DISCUSSION

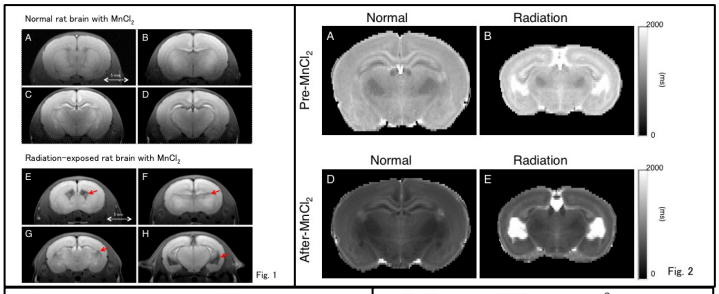

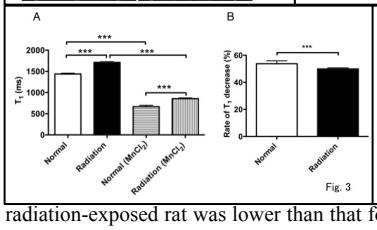

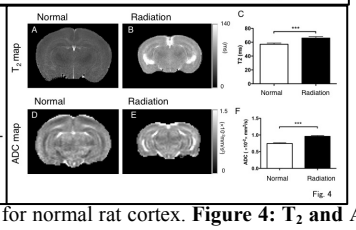

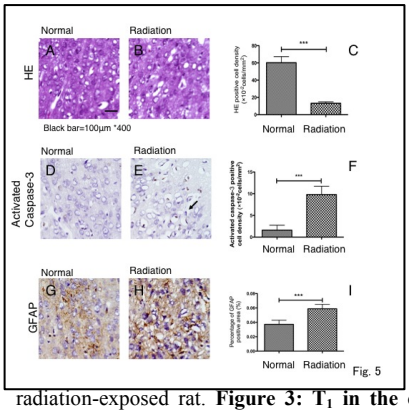

Figure 1: Typical T_1WI. Panels A, B, C and D: MEMRI of normal rat brain. Panels E, F, G and H: MEMRI of radiation-exposed rat. Red arrows indicate ventricle dilatation.

Figure 2: T_1-mapping. Typical coronal T_1-maps. (A) T_1-mapping prior to $MnCl_2$ administration for normal rat. (B) T_1-mapping prior to $MnCl_2$ administration for radiation-exposed rat. (D) T_1-mapping after $MnCl_2$ administration for normal rat. (E) T_1-mapping after $MnCl_2$ administration for radiation-exposed rat. **Figure 3: T_1 in the cortex**. (A) Cortical T_1 values after $MnCl_2$ administration. (B) The ratio of cortical T_1 before and after MnCl2 administration for radiation-exposed rat was significantly lower than that for normal rat ($p < 0.001$). This result suggests that the uptake of $MnCl_2$ in cortex for radiation-exposed rat was lower than that for normal rat cortex. **Figure 4: T_2 and ADC maps.** Typical T_2 and ADC maps for the 2WN and 2WR groups are presented. (A) Cortical T_2 for the 2WN animals was lower than in other brain areas such as the thalamus and amygdalate. In (B), cortical T_2 is similar to that in other brain areas such as thalamus and amygdalate. In (C), cortical T_2 is compared for the 2WN and 2WR groups ($p < 0.05$). ADC maps for the (D) 2WN and (E) 2WR groups are also shown . In (D), the cortical ADC values are lower than in other brain areas such as the thalamus and amygdalate. In (E), the cortical ADC values are similar to those in other brain areas. In (F), the cortical ADCs for 2WN and 2WR were 0.82 ± 0.05 and 1.03 ± 0.03 mm^2/s, respectively. The ADC for 2WR was significantly higher than for 2WN ($p < 0.001$). **Figure 5: HE, Activated Caspase-3 and GFAP histology.** The top row (A, B) presents HE stained histological slices of the cortex for each group. Cell-density in the radiation-exposed cortex (2WN) was significantly lower than in normal rat cortex (C, $p < 0.001$). The middle row (D, E) contains Activated Caspase-3 stained histological slices of the cortex. Many activated-Caspase-3-positive cells (an example is indicated by the arrow), were observed in the cortex for the 2WR group. The density of activated Caspase-3 for the radiation-exposed group increased significantly (F, $p < 0.001$). The bottom row (G, H) shows GFAP-stained histological slices in the cortex. The GFAP-positive area in the radiation-exposed rats was larger than for the normal animals (I, $p < 0.001$).

CONCLUSION

We found that: 1) decreased $MnCl_2$ uptake for radiation-exposed rats (as indicated by longer MEMRI T_1 (Fig. 3)) and increase of activated-Caspase-3-positive cells (Fig. 5F) imply a decrease of cell viability (apoptotic cytopathogenicity) after prenatal radiation exposure; 2) larger T_2 and ADC (Fig. 4) and reduction in the number of HE-positive cells (Fig. 5C) implies a decrease in CNS cell density after radiation exposure. Proliferation of astroglia was also observed (Fig. 5I). Kawai et al recently reported that proliferation of astroglia is the predominant mechanism behind MEMRI enhancement after focal brain ischemia [5]. In our prenatal radiation-exposure model, both proliferation of astroglia and decrease of cell density were observed (Fig. 5C, I). Therefore, we hypothesise that the decrease in cell number counteracts the proliferation of astroglia in the radiation-exposure model. In conclusion, quantitative T_1 mapping with MEMRI in combination with ADC and T_2 mapping provides comprehensive multifunctional information for the evaluation and diagnosis of prenatal radiation exposure.

REFERENCE [1] Janeczko K, Pawlinski R, Setkowicz Z, Ziaja M, Soltys Z, Ryszka A. Brain Res 1997; 770:237-241. [2] Pena LA.Cancer Res 2000; 60:321-327 [3] I. Aoki, Y.J. Wu, A.C. Silva, R.M. Lynch and A.P. Koretsky, Neuroimage 22 (2004) pp. 1046–1059 [4] Sun Xue-Zhi, Takahashi Sentaro, Journal of Radiation Research. 2002 [5] Kawai Y, Aoki I, et al, Neuroimage 2009 in press.

ACKNOWLEDGEMENT The authors would like to thank Jeff Kershaw, Sayaka Shibata and Takeo Shimomura for valuable assistance.